Reflection Effect in Close Binaries. IV. Limb Darkening of the Reflected Radiation Incident from an Extended Surface of the Secondary

A. Peraiah and M. Srinivasa Rao *Indian Institute of Astrophysics, Bangalore 560034*

Abstract. The law of limb darkening has been calculated when the atmosphere of the primary component is illuminated by the extended surface of the secondary component in a binary system. The specific intensities calculated at infinity show marked changes when the plane-parallel approximation is replaced by the assumption of spherical symmetry. The middle portions of the illuminated surface reflect maximum radiation while the innermost and outermost layers show lesser amount of reflected radiation.

Key words: reflection effect—limb darkening

1. Introduction

It is customary to assume a law of limb darkening (see Kitamura 1954; Kopal 1959; Peraiah 1970) which is based on blackbody considerations. It is necessary to actually calculate the distribution of radiation field and then derive the law of limb darkening. In paper 2 of this series, the law of limb darkening was calculated as observed at infinity. It was assumed that the incident radiation was emitted by a point source. The self-radiation of the component had been estimated by using plane-parallel and spherically-symmetric approximations for the sake of comparison. Large differences occur in the radiation received at infinity when the above two approximations are employed. This encourages one to proceed further to investigate the radiation field received at infinity when the incident radiation comes from an extended surface of the secondary instead of a point source.

2. Computational procedure

The geometry of the model is shown in Fig. l(a). O and O′ are the centres of the primary and secondary respectively. The atmosphere of the primary is divided into several shells. We would like to calculate the effect of irradiation from the secondary on the

distribution of radiation field in the part of the atmosphere of the primary facing the secondary. We have considered a set of rays along the line of sight and tangential to the shell boundaries at points where the axis OO' intersect them. We estimate the radiation field at points such as P where the parallel rays meet the shell boundaries. The radiation field at P is calculated by estimating the source function at P due to the radiation incident at P from the surface SW of the secondary facing the primary. We have selected a number of rays from SW incident on the atmosphere and entering the surface at points such as T, τ etc. We intend to calculate the ray paths PT, Pτ etc., and optical depths along these rays. The segments such as Pτ in $\lfloor$TPT$_1$ are given by

$$\text{P}\tau = \text{OP}\left(A\frac{B'}{B} + A'\right) \tag{1}$$

Where

$$B = \frac{\text{OP}}{\text{OT}}A, \qquad B' = (1 - B^2)^{\frac{1}{2}},$$

$$A = \xi\eta' - \xi'\eta, \qquad A' = (1 - A^2)^{\frac{1}{2}},$$

$$\eta = \sin E = \frac{\text{SE}}{\text{PE}}, \qquad \eta' = \cos E,$$

$$\xi = abc + a'b'c + a'bc' - ab'c', \qquad \xi' = (1 - \xi^2)^{\frac{1}{2}},$$

$$a = \text{OQ}/\text{OP}, \qquad a' = (1 - a^2)^{\frac{1}{2}},$$

$$b = \text{PS}/\text{O'P}, \qquad b' = (1 - b^2)^{\frac{1}{2}},$$

$$c = \text{PQ}/\text{O'P}, \qquad c' = (1 - c^2)^{\frac{1}{2}}.$$

Similarly the segments such as Pτ in $\lfloor$T$_1$PT$_2$ are given by

$$\text{P}\tau' = \text{OP}\left[\mu\left(\frac{s'}{s}\right) + \mu'\right], \tag{2}$$

where

$$\mu = v'\Delta + \Delta'v, \qquad \mu' = (1 - \mu^2)^{\frac{1}{2}},$$

$$s = \frac{\text{OP}}{\text{OT}}\mu, \qquad s' = (1 - s^2)^{\frac{1}{2}},$$

$$v = \frac{\text{WE}'}{\text{PE}'}, \qquad v' = (1 - v^2)^{\frac{1}{2}},$$

$$\text{PE}' = (\text{PW}^2 + \text{WE}'^2)^{\frac{1}{2}}, \qquad \Delta = \xi(1 - 2\delta^2) - 2\xi'\delta\delta',$$

$$\Delta' = (1 - \Delta^2)^{\frac{1}{2}}, \qquad \delta = \frac{\text{SO}'}{\text{PO}'},$$

$$\delta' = (1 - \delta^2)^{\frac{1}{2}}.$$

For a given density distribution, we can calculate the optical depth along the segments such as Pτ and Pτ'. Using these optical depths, the specific intensities and source

functions at the point P due to irradiation from the secondary can be calculated. The boundary conditions and the method of calculation have been described in paper III of this series. We solve the equation of radiative transfer in spherical symmetry and obtain the source function S_s due to self radiation. Here we have calculated the optical depth according to $1/r^2$ law of variation of electron density and assumed isotropic scattering by electrons. The total source function S_T is the sum of the source functions due to self radiation S_s and irradiation S_I:

$$S_T = S_S + S_I \tag{3}$$

We thus calculate the set of source functions at the points of intersection of the ray parallel to the line of sight and the shell boundaries. These source functions are used to calculate the emergent specific intensities at infinity by using the formula

$$I_{n+1}(r) = I_0(n) \exp(-\tau)^+ \int_0^\tau S_T(t) \exp[-(\tau - t)]dt, \tag{4}$$

where $I_n(r)$ corresponds to the specific intensity of the ray passing between shell numbers η and $n + 1$ corresponding to perpendicular radial distance r, along the axis OO′. $I_0(n)$ corresponds to the incident intensity at the boundary of the shell and τ is the optical depth in the sector along the ray path. The source function $S_T(t)$ is calculated by linear interpolation between $S_T(n)$ and $S_T(n + 1)$. The specific intensity at the boundary of each shell is calculated by using Equation (4).
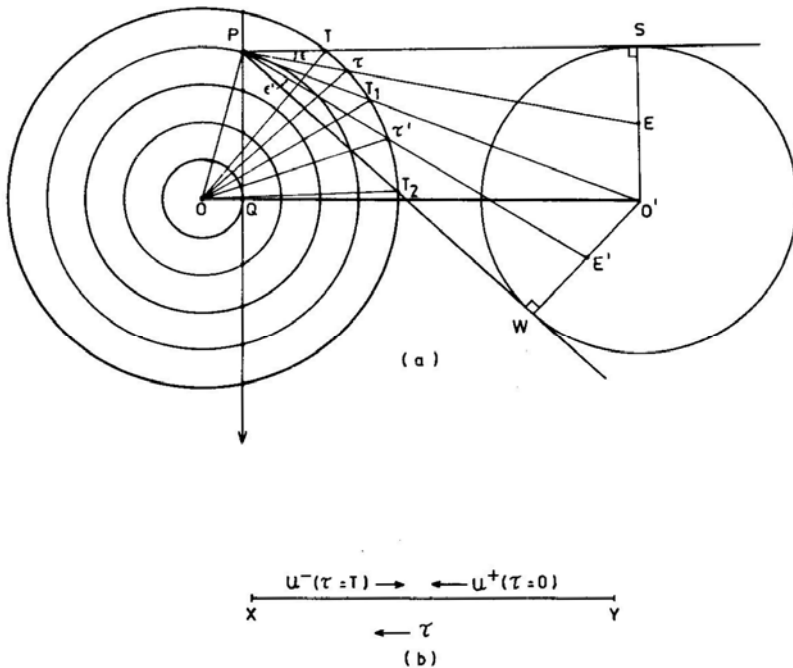

Figure 1. (a) Schematic diagram of the model of reflection of radiation from the extended surface of the secondary. (b) Schematic diagram of the Rod model. U_+ and u_- are the specific intensities in the opposite directions.

3. Results and discussion

In Fig. l (a), we have given the schematic diagram of the model. We have divided the atmosphere into 25 shells. The line of sight is in the direction of PQ. We have calculated the source functions at the points where PQ meets the shell boundaries. It must be noted that the configuration shown in Fig. 1 (a) in this paper is different from Fig. 1 (a) of Paper 3. We are considering here the radiation along the line of sight whereas in the earlier case, we calculated the radiation field along the radius vector. Therefore one need not look for similarities. In Fig. l (b) we show the rod model. In Fig. 2, the source functions due to reflection are plotted. Shell number 1 has its inner boundary at the point Q; the outer boundary of the shell number 25 coincides with that of the outer boundary of the atmosphere. We have assumed a $1/r^2$ law of density variation, with a density of 10^{13} cm^{-3} at Q. The total radial optical depth reaches a maximum of 4; along the line of sight it varies between 0 and 5 from outermost layer to the innermost layer at Q, depending upon the perpendicular distance of the ray path from O along the axis OO′. The source functions S_1 at points of intersection of the axis OO′ and shell boundaries are plotted in Fig. 2(a), for different values of I, the ratio of the radiations of
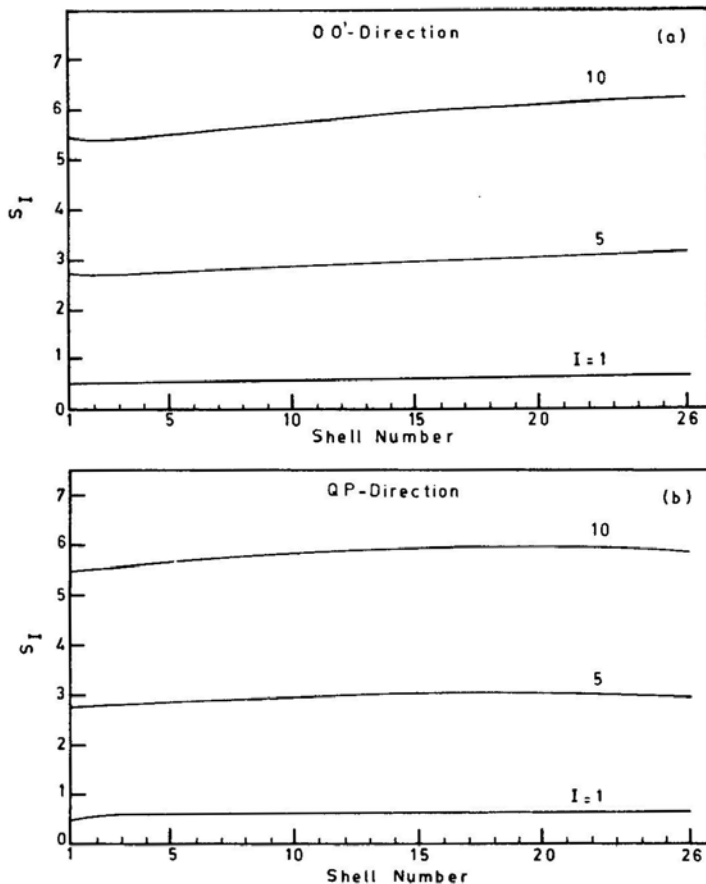

Figure 2. The source functions S_I due to reflection in (a) OO′ direction and (b) QP direction. S_1 is given in arbitrary units.

the two components (see Paper 3). We notice that the source functions are almost linear and increase with the shell numbers, *i.e.*, towards the secondary component from whose surface the primary is receiving the incident radiation. This can be understood easily on physical grounds. However, the increase is not as big as one expects because of the fact that the density falls as $1/r^2$ towards the outer layers of the atmosphere. The source functions S_I (due to incident radiation from the secondary component) along the line of sight QP (tangent to the star's surface) are plotted against the shell numbers in Fig. 2(b). The behaviour of S_I here, is slightly different from that of Fig. 2(a). It increases slowly towards P and then starts falling. This can be understood on the basis that the incident radiation, on reaching points such as P which are away from the centre of the star, is weakened by the cosine factor.

Compare Fig. 2 with Fig. 3 of Paper 3. Here we have plotted the source function due to irradiation only, whereas in the earlier case, we had plotted the total source function
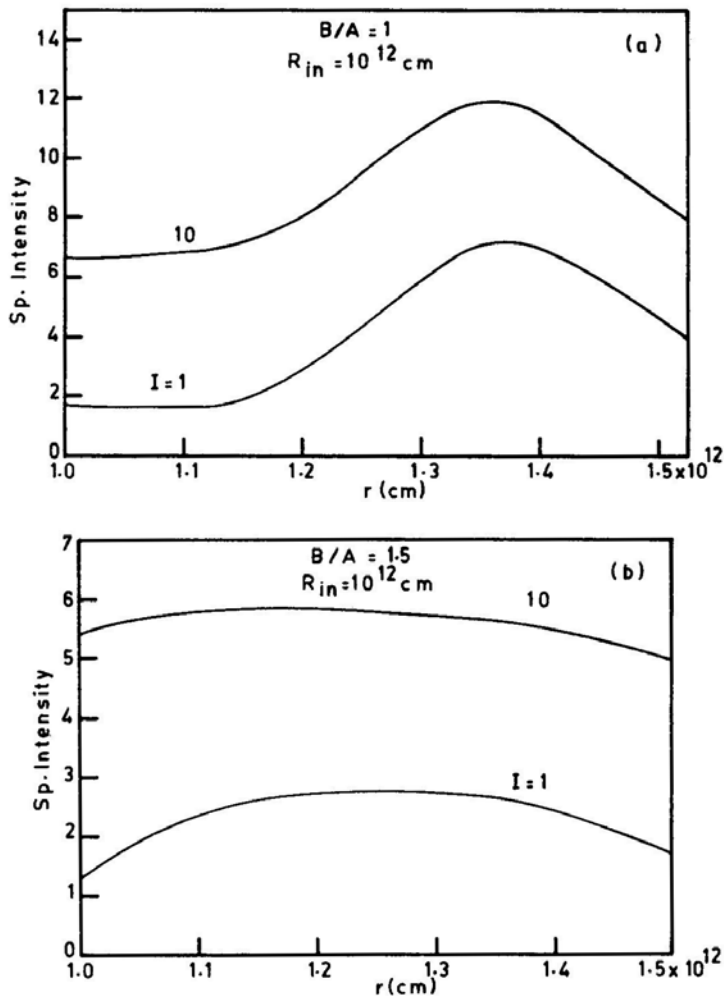

Figure 3. Variation of specific intensity from centre to limb is given in arbitrary units with (a) plane-parallel geometry ($B/A = 1$) and (b) spherical geometry ($B/A = 1.5$), where B and A are the outer and inner radii of the atmosphere ($R_{in} = 10^{12}$ cm).

$(S_I + S_s)$. The specific intensity along the line of sight is given in Figs 3–5. The results given in Fig. 3 refer to those of plane-parallel (a) and spherically-symmetric (b) approximations. This means that the source function S_s due to self-radiation is calculated using the above two geometrical stratifications, while the source function S_I due to incident radiation remains the same in both the cases. The source function in
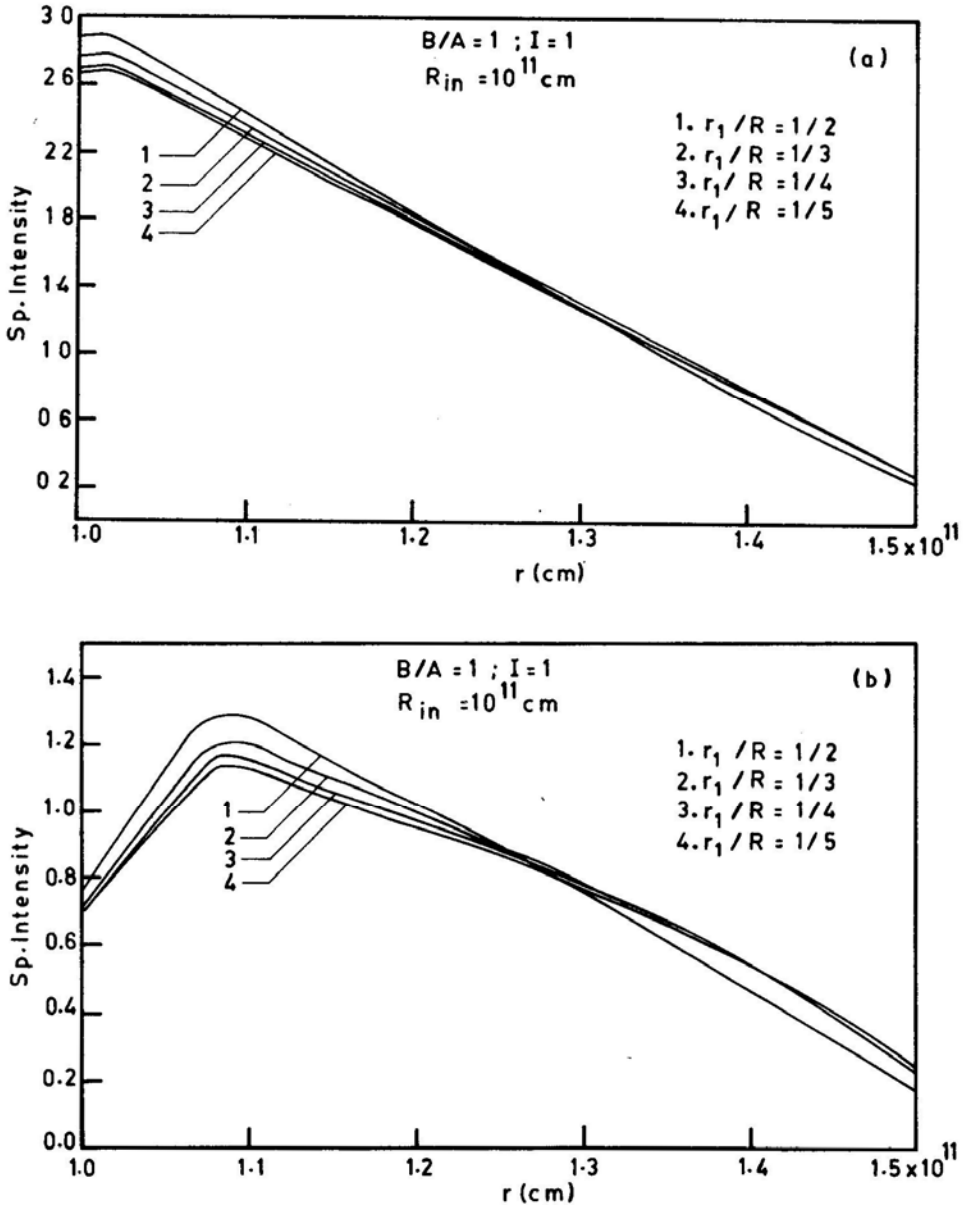

Figure 4. Variation of specific intensities from centre to limb in (a) plane-parallel geometry and (b) spherically symmetric geometry, for $I = 1$ and $R_{in} = 10^{11}$ cm. The results are given for different values of r_1/R, where r_1 is the outer radius of the star and R is the separation between the centres of the two components.
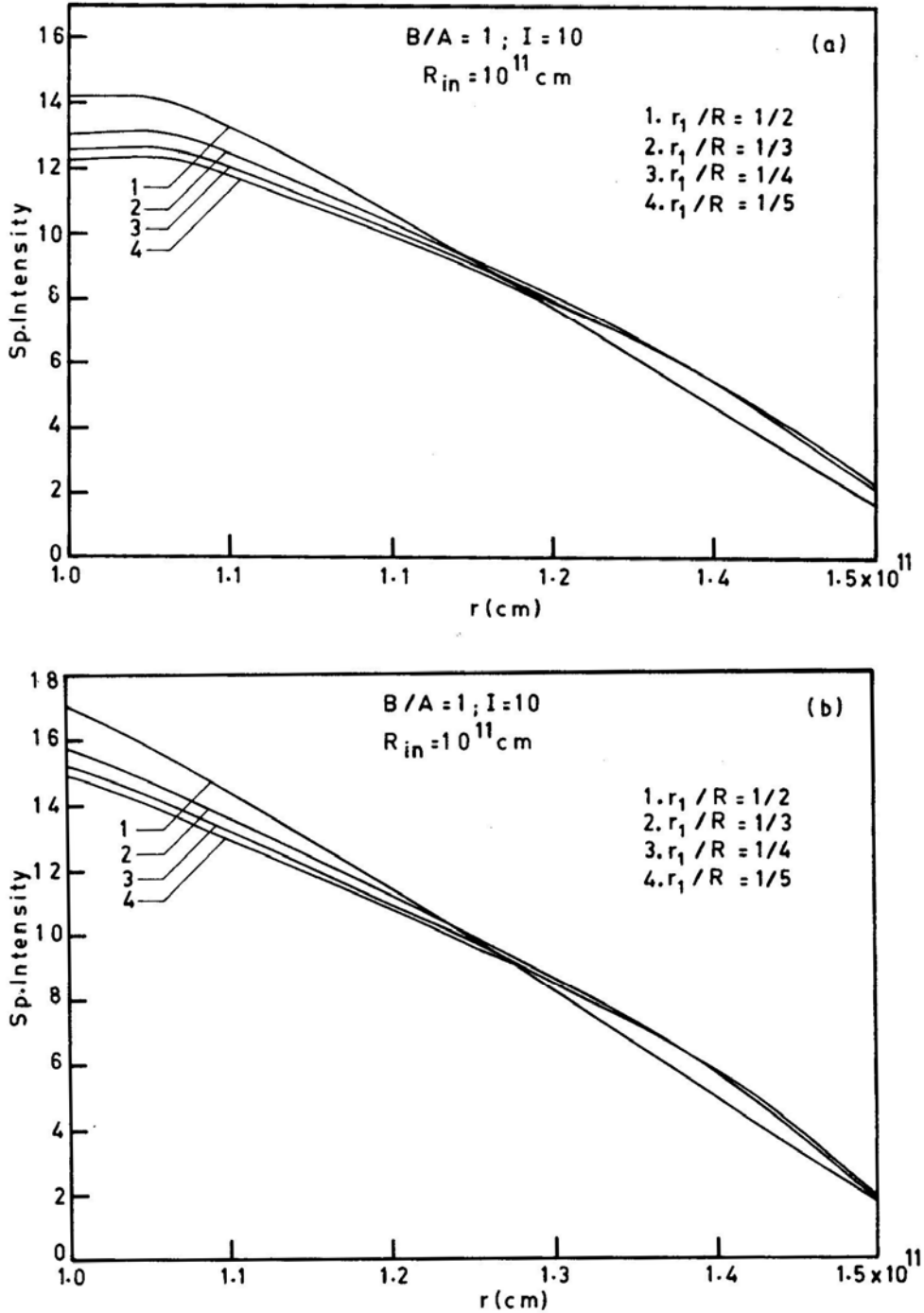
Figure 5. Variation of specific intensities from centre to limb in (a) plane-parallel geometry and (b) spherically symmetric geometry, for $I = 10$ and $R_{in} = 10^{11}$ cm.

Plane-parallel approximation is obtained from the solution of the radiative transfer equation without the term,

$$\frac{1}{r}\frac{\partial}{\partial\mu}\left[(1-\mu^2)u(r,\mu)\right].$$

We have calculated the optical depth in spherical and plane-parallel approximations by assuming the same electron density distribution. We have considered an atmosphere whose thickness is one-half of the stellar radius in calculating the source function due to self radiation. The results given in Fig. 3(a)and (b)show different types of variations in the specific intensities from $r = r_{in}$ to $r = r_{out}$ In plane-parallel stratification, the intensities remain constant until some point and then reach a maximum at $r \simeq 1.35 \times 10^{12}$ cm. From here onwards, the intensities fall as one approaches the outer surface of the atmosphere. In the case of spherical geometry, the intensities increase slightly and then decrease towards the outer surface. The law of variation of the intensities from centre to limb is different in the two approximations. Although the extension of the atmosphere is only one half of the stellar radius, the differences are quite large. Therefore, one must always use the assumption of spherical symmetry even when the atmosphere is small compared to the stellar radius. In Fig. 4, we have plotted the variation of specific intensities from centre to limb for $R_{in} = 10^{11}$ cm, $I = 1$, for various values of r_1/R, where r_1 is the outer radius of the star and R is the distance between the centres of the two stars. In plane-parallel approximation, the law of variation of specific intensities is almost linear and falls rapidly towards the surface, whereas in the case of spherical symmetry, the specific intensities reach a maximum and then fall. The results given in Fig. 5 show a trend similar to those given in Fig. 4. The law of limb darkening does not seem to depend much on the ratio r_1/R .

   We have shown in this paper that the law of variation of radiation from centre to limb depends considerably on whether one considers plane-parallel or spherically symmetric geometry and also on the distribution of electron density.

References

Kitamura, M. 1954, *Publ astr. Soc. Japan,* **5,** 114.
Kopal, Z. 1959, *Close Binary Systems,* John Wiley, New York.
Peraiah, A. 1970, *Astr. Astrophys.,* **7,** 473.
Peraiah, A. 1983, *J. Astrophys. Astr.,* **4,** 11 (Paper 2).
Peraiah, A. 1983, *J. Astrophys. Astr.,* **4,** 151 (Paper 3).